Mutual Calibration of Multiple Current Sensors with Accuracy Uncertainties in IPMSM Drives for Electric Vehicles

Jiadong Lu, *Member, IEEE*, Yihua Hu, *Senior Member, IEEE,* Guipeng Chen, *Member, IEEE*, Zheng Wang, *Senior Member, IEEE,* and Jinglin Liu, *Member, IEEE*

Abstract—**This paper proposes a mutual calibration strategy for multiple current sensors in an electric vehicle motor drive. The motor drive usually consists of three current sensors, i.e., a DC-bus current sensor and two phase current sensors. Due to the aging effect and harsh operating environment, the accuracy uncertainty issue is inevitable in these crucial sensors, which results in poor driving performance. In this paper, the detection voltage injection (DV-Injection) method is proposed for mutual calibration of the aforementioned current sensors. Two opposite basic vectors are set together to detect and eliminate the offset error of the DC-bus current sensor. Then, both the directly measured phase-current values by the phase-current sensors and the indirectly measured values by the DC-bus current sensor are sampled. These values are utilized for mutual calibration of the phase-current sensor offset errors and scaling error differences among all the current sensors. Meanwhile, the DV-Injection process is only applied in the period of calibration process, whereas in the remaining intervals the space vector pulse width modulation (SVPWM) technology is utilized. Finally, the effectiveness of the proposed scheme is verified by simulation study in Matlab/Simulink and experimental results on a 5kW IPMSM motor prototype.**

Index Terms—**Accuracy uncertainty, error compensation, interior permanent magnet synchronous motor (IPMSM), mutual calibration.**

I. INTRODUCTION

ELECTRIC vehicles (EVs) are typically the large-scale power applications that operate under harsh conditions,

J. Lu and J. Liu are with the School of Automation, Northwestern Polytechnical University (NWPU) and Yangtze River Delta Research Institute of NWPU, Xi'an 710129, China. (E-mail: j.d.lu@nwpu.edu.cn, jinglinl@nwpu.edu.cn).
Y. Hu is with the Department of Electrical Engineering and Electronics, University of Liverpool, Liverpool L69 3GJ, U.K. (E-mail: y.hu35@liverpool.ac.uk) *(Corresponding author).*
G. Chen is with the School of Aerospace Engineering, Xiamen University, China. (E-mail: cgp2017@xmu.edu.cn).
Z. Wang is with the School of Electrical Engineering, Southeast University, Nanjing 210096, China. (E-mail: zwang@eee.hku.hk).
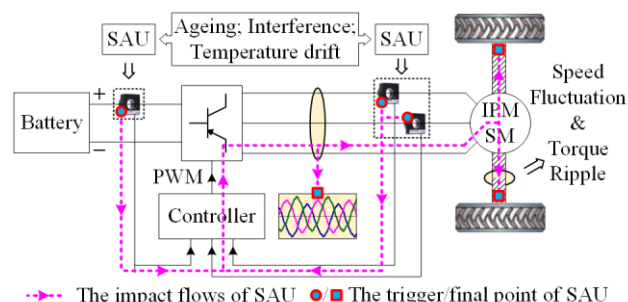

Fig. 1. Typical IPMSM drive with current SAU.

where high reliability is of paramount significance, especially for the future manless ones [1], [2]. Due to the outstanding features of interior permanent magnet synchronous motors (IPMSMs), they show good prospects in the fields of EV applications [3]-[5]. In order to effectively control IPMSM in EVs, several current sensors are installed for each motor drive to provide the feedback signals for the micro-controller as illustrated in Fig.1 [6], [7]. By good design, the drive achieves excellent performance at the beginning [8]. However, after a long time of use, the accuracy of the multiple current sensors inevitably degrades with different degrees because of ageing, interference and temperature drift [9]-[11]. For the sake of expressing this issue conveniently, it is defined as sensor accuracy uncertainty (SAU), because the degree of inaccuracy for each sensor is unknown. In the case of current SAU, as shown in Fig.1, inaccurate current feedback signals may be produced, resulting in undesirable speed fluctuation, torque ripple, and unbalanced three-phase currents [12], [13]. Besides, it is difficult to determine which sensor is seriously inaccurate. Furthermore, the situation that the multiple current sensors are not completely accurate, but all the sensors are in relatively healthy conditions can be encountered, making it unreasonable to replace or repair any of these sensors. However, if the sensor inaccuracy is not calibrated, the service lifetime of EV will be reduced due to the deteriorated system performance, making it impossible to meet the expected lifetime of at least 10 years [14]. As the driving force and speed are both controlled by the system, the deteriorated performance may affect the driving experience, and even lead to danger [10], [12], [15]. The SAU issue also brings great challenges to the pilotless technologies.

A typical IPMSM drive with current SAU is illustrated in Fig.1 [16]. The drive consists of two phase current sensors and

one DC-bus current sensor. These high-precision current sensors are installed to provide accurate current feedback signals, which are very important for the normal and efficient operation of the drive [17], [18]. However, measurement inaccuracy of these current sensors may appear considering ageing, interference and temperature drift. As the factors that affect the measurements are complex, a thorough solution is not easy to obtain. More specifically, in practice, different degrees of inaccuracy usually occurs in these sensors, instead of the case that only one sensor totally breaks down with others being intact. Therefore, it is necessary to propose a mutual calibration strategy for multiple current sensors with SAU in EVs.

Although many solutions have been proposed to solve the current sensor fault issue [19]-[27], they all focused on the faults in one or two sensors. A continuous drive operation strategy that excludes the sensor faults is proposed in [28], which comprises of two higher-order sliding mode observers and one Luenberger observer, making the fault detection process complicated. In addition, all these literature focus on the cases that at least one sensor fails. In fact, however, the more commonly encountered scenario is that the sensors do not completely fail, while they are able to continue working with uncertainties in the measurement accuracy. In this case, a rational solution is using these sensors as usual, whereas real-time accuracy assessment and compensation are required [10]-[13]. In [26], [27] the impacts of sensor errors on the system performance are analyzed in detail. For the case that accuracy uncertainties only exist in one phase current sensor and the position sensor, in [10], a new scheme for detection, isolation, and compensation strategy was proposed. However, this scheme will be invalid if the currents derived by both the two current sensors are erroneous. In other words, in the case that SAU exists in multiple sensors (i.e., two phase current sensors with SAU), the approach proposed in [10] is not valid anymore. The current sensor error compensation strategies in voltage source inverter (VSI) drives are studied in [11]-[13], [29], where the sensor currents are estimated from the information of the output voltage. However, several digital filters and complicated computing algorithms are utilized in the strategy, making it difficult to implement.

In this paper, the accuracy uncertainties of multiple current sensors are analyzed, where the DC-offset and scaling errors are compensated with a mutual calibration strategy. For the proposed multiple current sensor error compensation strategy, a completely healthy sensor is not required, which means that the proposed strategy is still effective when none of the current sensors is healthy. The proposed strategy is based on the relationship between the DC-bus current and the three-phase currents with different switching states. It should be pointed out that the proposed mutual calibration strategy of current sensor errors does not rely on any of the complicated digital filters and is independent of the motor parameters. Furthermore, the algorithm is simple for implementation.

This paper is organized as follows. In Section II, the offset error calibration strategy of DC-bus current sensor is illustrated. In Section III, the mutual calibration strategies of the offset errors in phase-current sensors and the scaling error differences

TABLE I
THE RELATIONSHIP BETWEEN DC-BUS AND THREE-PHASE CURRENTS.

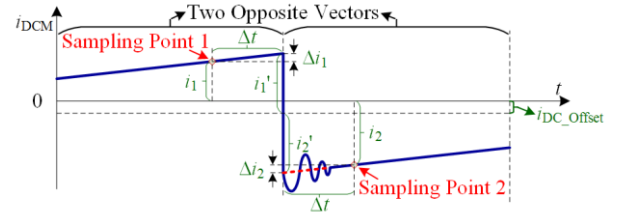| Vector	V_{000} (V_0)	V_{100} (V_1)	V_{110} (V_2)	V_{010} (V_3)	V_{011} (V_4)	V_{001} (V_5)	V_{101} (V_6)	V_{111} (V_7)
i_{DC}	0	i_A	$-i_C$	i_B	$-i_A$	i_C	$-i_B$	0

Fig. 2. The measured DC-bus current i_{DCM} under two opposite vectors.

among all the current sensors are proposed. In Section IV, the overall control strategies are illustrated. In Section V and VI, simulation and experimental results are presented, respectively. The conclusion is given finally in Section VII.

II. SELF-CALIBRATION STRATEGY FOR DC-BUS CURRENT SENSOR OFFSET ERROR

Offset and scaling errors are the most common error types of a current sensor [10]. However, the errors of multiple current sensors are different due to modulation and specificity. As illustrated in Fig.1, a DC-bus current sensor is usually installed for overcurrent protection. In this paper, further utilization of the DC-bus current sensor will be carried out for phase-current sensor mutual calibration. However, a self-calibration scheme must be applied for the DC-bus current sensor first to ensure accurate DC-bus current measurement. The DC-bus current i_{DC} is related to the three-phase currents i_A, i_B, and i_C according to different switching states as displayed in Table I. It can be seen that the values of i_{DC} under any two opposite vectors (V_1 and V_4; V_3 and V_6; V_2 and V_5) are opposite to each other. Therefore, if the sum of the two values is not zero, the offset error of the DC-bus current sensor is detected. However, the DC-bus current value changes all the time due to the current chopping effect. In order to effectively detect the offset error, the two opposite vectors are set together. The time interval Δt between the junction point and one of the two measuring points should be equal to that between the junction point and the other measuring point, as illustrated in Fig.2.

In Fig.2, if the offset error i_{DC_Offset} does not exist in the DC-bus current sensor, the two sampled currents i_1 and i_2 have opposite values to each other when Δi_1 is equal to Δi_2. However, if i_{DC_Offset} is not zero, it can be detected as the average value of i_1 and i_2. The precondition of applying this strategy is that the values of two current increments Δi_1 and Δi_2 are the same, which implies that the current slope $\Delta i_1/\Delta t$ is equal to $\Delta i_2/\Delta t$.

The mathematical model of IPMSM is given in [30]

$$\begin{bmatrix} u_\alpha \\ u_\beta \end{bmatrix} = R \cdot \begin{bmatrix} i_\alpha \\ i_\beta \end{bmatrix} + \begin{bmatrix} L_0 + L_2\cos2\theta & L_2\sin2\theta \\ L_2\sin2\theta & L_0 - L_2\cos2\theta \end{bmatrix} \times \frac{d}{dt}\begin{bmatrix} i_\alpha \\ i_\beta \end{bmatrix}$$
$$+ \frac{d\theta}{dt}\left(2L_2\begin{bmatrix} -\sin2\theta & \cos2\theta \\ \cos2\theta & \sin2\theta \end{bmatrix}\begin{bmatrix} i_\alpha \\ i_\beta \end{bmatrix} + \psi_f\begin{bmatrix} -\sin\theta \\ \cos\theta \end{bmatrix}\right) \quad (1)$$

$$\begin{bmatrix} L_0 \\ L_2 \end{bmatrix} = \frac{1}{2} \begin{bmatrix} 1 & 1 \\ 1 & -1 \end{bmatrix} \cdot \begin{bmatrix} L_d \\ L_q \end{bmatrix} \quad (2)$$

where u_α, u_β and i_α, i_β are the motor voltages and currents in the α-β axis frame, respectively; R denotes the motor resistance; θ represents the rotor angle; ψ_f is the permanent magnet flux linkage; L_d and L_q are the inductance in the d-q axis frame.

When considering the current chopping effect, u_α and u_β in (1) are no longer the voltage vectors to be synthesized. In fact, u_α and u_β denote the instantaneous voltages on the motor windings, which are related to the switching states (action vectors) and are displayed in Table II. In the table, u_{A_Ins}, u_{B_Ins}, u_{C_Ins}, u_{α_Ins} and u_{β_Ins} are the instantaneous voltages. U_{DC} is the DC-bus voltage. In this case, the first and third items in (1) can be neglected

$$\begin{bmatrix} u_{\alpha\_Ins} \\ u_{\beta\_Ins} \end{bmatrix} = \begin{bmatrix} L_0 + L_2 \cos 2\theta & L_2 \sin 2\theta \\ L_2 \sin 2\theta & L_0 - L_2 \cos 2\theta \end{bmatrix} \times \frac{d}{dt} \begin{bmatrix} i_{\alpha\_Ins} \\ i_{\beta\_Ins} \end{bmatrix} \quad (3)$$

The current slopes can be obtained

$$\frac{d}{dt} \begin{bmatrix} i_{\alpha\_Ins} \\ i_{\beta\_Ins} \end{bmatrix} = \frac{1}{L_d L_q} \begin{bmatrix} L_0 - L_2 \cos 2\theta & -L_2 \sin 2\theta \\ -L_2 \sin 2\theta & L_0 + L_2 \cos 2\theta \end{bmatrix} \cdot \begin{bmatrix} u_{\alpha\_Ins} \\ u_{\beta\_Ins} \end{bmatrix} \quad (4)$$

Finally, the three-phase instantaneous current slopes (di_{A_Ins}/dt, di_{B_Ins}/dt, and di_{C_Ins}/dt) can be derived from (4) by 2/3 transform as shown in (5)-(7) and Table III.

$$\frac{d}{dt} \begin{bmatrix} i_{A\_Ins} \\ i_{B\_Ins} \\ i_{C\_Ins} \end{bmatrix} = \mathbf{L} \cdot \begin{bmatrix} u_{A\_Ins} \\ u_{B\_Ins} \\ u_{C\_Ins} \end{bmatrix} \quad (5)$$

$$\mathbf{L} = \frac{2}{3 L_d L_q} \cdot \begin{bmatrix} l_1 & -\dfrac{l_1}{2} + \dfrac{\sqrt{3}l_3}{2} & -\dfrac{l_1}{2} - \dfrac{\sqrt{3}l_3}{2} \\ -\dfrac{l_1}{2} + \dfrac{\sqrt{3}l_3}{2} & \dfrac{l_1}{4} + \dfrac{3l_2}{4} - \dfrac{\sqrt{3}l_3}{2} & \dfrac{l_1}{4} - \dfrac{3l_2}{4} \\ -\dfrac{l_1}{2} - \dfrac{\sqrt{3}l_3}{2} & \dfrac{l_1}{4} - \dfrac{3l_2}{4} & \dfrac{l_1}{4} + \dfrac{3l_2}{4} + \dfrac{\sqrt{3}l_3}{2} \end{bmatrix} \quad (6)$$

$$\begin{cases} l_1 = L_0 - L_2 \cos 2\theta \\ l_2 = L_0 - L_2 \cos 2\theta \\ l_3 = L_2 \sin 2\theta \end{cases} \quad (7)$$

From Table III, it can be seen that the current slopes of i_{DC} under any two opposite action vectors are all the same, which demonstrates the two current slopes $\Delta i_1/\Delta t$ and $\Delta i_2/\Delta t$ are the same in Fig.2. Therefore, the increments of the two currents Δi_1 and Δi_2 are proven to be the same. In this case, the average value of i_1 and i_2 in Fig.2 can be utilized for DC-bus current sensor offset error detection and compensation.

It should be noted that even if the first and third items in (1) are not small enough to be ignored, they have little effect on the

TABLE II
THE INSTANTANEOUS VOLTAGES ACTING ON THE MOTOR WINDINGS.

V_X	V_1	V_2	V_3	V_4	V_5	V_6
u_{A_Ins}	$2U_{DC}/3$	$U_{DC}/3$	$-U_{DC}/3$	$-2U_{DC}/3$	$-U_{DC}/3$	$U_{DC}/3$
u_{B_Ins}	$-U_{DC}/3$	$U_{DC}/3$	$2U_{DC}/3$	$U_{DC}/3$	$-U_{DC}/3$	$-2U_{DC}/3$
u_{C_Ins}	$-U_{DC}/3$	$-2U_{DC}/3$	$-U_{DC}/3$	$U_{DC}/3$	$2U_{DC}/3$	$U_{DC}/3$
u_{α_Ins}	$\sqrt{6}U_{DC}/3$	$U_{DC}/\sqrt{6}$	$-U_{DC}/\sqrt{6}$	$-\sqrt{6}U_{DC}/3$	$-U_{DC}/\sqrt{6}$	$U_{DC}/\sqrt{6}$
u_{β_Ins}	0	$U_{DC}/\sqrt{2}$	$U_{DC}/\sqrt{2}$	0	$-U_{DC}/\sqrt{2}$	$-U_{DC}/\sqrt{2}$

TABLE III
THE VALUES OF THREE-PHASE INSTANTANEOUS CURRENT SLOPES.

Vector	V_1	V_2	V_3	V_4	V_5	V_6
di_{A_Ins}/dt	Q_1	$-Q_5$	Q_4	$-Q_1$	Q_5	$-Q_4$
di_{B_Ins}/dt	Q_4	Q_6	Q_2	$-Q_4$	$-Q_6$	$-Q_2$
di_{C_Ins}/dt	Q_5	$-Q_3$	$-Q_6$	$-Q_5$	Q_3	Q_6
di_{DC}/dt	Q_1	Q_3	Q_2	Q_1	Q_3	Q_2

Q_1	$z[L_0 - L_2\cos 2\theta]$	Q_4	$z[-L_0/2 - L_2\sin(2\theta-\pi/6)]$
Q_2	$z[L_0 + L_2\sin(2\theta+\pi/6)]$	Q_5	$z[-L_0/2 + L_2\sin(2\theta+\pi/6)]$
Q_3	$z[L_0 - L_2\sin(2\theta-\pi/6)]$	Q_6	$z[L_0/2 + L_2\cos 2\theta]$
$z = 2U_{DC}/(3L_d L_q)$			

TABLE IV
THE RELATIONSHIP BETWEEN THE MEASURED DC-BUS CURRENT AND ACTUAL THREE-PHASE CURRENTS.

Vector	V_{100} (V$_1$)	V_{110} (V$_2$)	V_{010} (V$_3$)	V_{011} (V$_4$)	V_{001} (V$_5$)	V_{101} (V$_6$)
i_{DCM_SCA}	$k_{DC} i_A$	$-k_{DC} i_C$	$k_{DC} i_B$	$-k_{DC} i_A$	$k_{DC} i_C$	$-k_{DC} i_B$

proposed calibration method. Because Δt is usually very short (a few microseconds), Δi_1 and Δi_2 are also very small.

III. MUTUAL CALIBRATION STRATEGY FOR MULTIPLE CURRENT SENSOR ERRORS

The aforementioned two error types - offset error and scaling error in the phase current sensors have extremely negative effects on the drive [10]. Usually, the three-phase currents for a three-phase three-wire system are detected by two phase current sensors, and the current in the third phase is obtained by the Kirchhoff's current law ($i_A + i_B + i_C = 0$). Assume that the actual three-phase currents are i_A, i_B, and i_C, the measured three-phase currents are i_{AM}, i_{BM}, and i_{CM}. The errors can be expressed as

$$\begin{cases} i_{AM} = k_A \cdot i_A + i_{A\_Offset} \\ i_{BM} = k_B \cdot i_B + i_{B\_Offset} \\ i_{CM} = -i_{AM} - i_{BM} \end{cases} \quad (8)$$

where k_A, k_B and i_{A_Offset}, i_{B_Offset} indicate the scaling and offset errors of phase-A, B current sensors.

A. Mutual Calibration of the Offset Errors in the Phase Current Sensors

In the previous part, the offset error of DC-bus current sensor has been calibrated, and the DC-bus current without the offset error, i.e., i_{DCM_SCA} is illustrated in Table IV.

From (8) and Table IV, it can be seen that the offset errors of the phase current sensors (i_{A_Offset} or i_{B_Offset}) can be detected according to two sets of sampled current values. Take i_{A_Offset} as

an example, the actual phase-A current values are i_{A1} and i_{A2}; the measured phase-A current values (by phase-A current sensor, i_{AM}) are i_{AM1} and i_{AM2}; the reconstructed phase-A current values (by DC-bus current sensor, i_{DCM_SCA}) are i_{ARE1} and i_{ARE2}

$$\begin{cases} i_{AM1} = k_A \cdot i_{A1} + i_{A\_Offset} \\ i_{AM2} = k_A \cdot i_{A2} + i_{A\_Offset} \end{cases} \tag{9}$$

$$\begin{cases} i_{ARE1} = k_{DC} \cdot i_{A1} \\ i_{ARE2} = k_{DC} \cdot i_{A2} \end{cases} \Leftrightarrow \begin{cases} i_{A1} = i_{ARE1}/k_{DC} \\ i_{A2} = i_{ARE2}/k_{DC} \end{cases} \tag{10}$$

By substituting (10) into (9), the offset error of the phase-A current sensor can be finally obtained

$$i_{A\_Offset} = \left(i_{ARE1} \cdot i_{AM2} - i_{ARE2} \cdot i_{AM1}\right)/\left(i_{ARE1} - i_{ARE2}\right) \tag{11}$$

The offset error of the phase-B current sensor i_{B_Offset} can be obtained by the same method

$$i_{B\_Offset} = \left(i_{BRE1} \cdot i_{BM2} - i_{BRE2} \cdot i_{BM1}\right)/\left(i_{BRE1} - i_{BRE2}\right) \tag{12}$$

where i_{BM1}, i_{BM2} and i_{BRE1}, i_{BRE2} are the corresponding phase-B variables to those defined in phase-A current sensor.

It is worth noting that the proposed mutual offset error calibration strategy for the phase current sensors is also applicable for the three-phase current sensor based systems.

B. Mutual Calibration of the Scaling Error Differences Among the Phase Current Sensors

Upon the mutual calibration of the multiple phase current sensors, the detected DC-bus and three-phase current values can be expressed as

$$\begin{cases} i_{DCM\_SCA} = k_{DC} \cdot i_{DC} \\ i_{AM\_SCA} = k_A \cdot i_A \\ i_{BM\_SCA} = k_B \cdot i_B \\ i_{CM\_SCA} = -k_A \cdot i_A - k_B \cdot i_B \end{cases} \tag{13}$$

where i_{AM_SCA}, i_{BM_SCA}, i_{CM_SCA} are the three-phase currents without the offset errors.

The scaling error differences among the phase current sensors cause the speed ripple of two times the fundamental stator current frequency [12]. In order to compensate the scaling errors among the phase current sensors, the DC-bus current sensor is utilized. This is because the DC-bus current sensor has certain relationships with all the phase currents, which builds up a link between the phase current sensors.

The actual phase-A and -B current values are i_A and i_B; the measured phase-A and -B current values (by phase current sensors, i_{AM_SCA}, i_{BM_SCA}) are i_{AM} and i_{BM}; the reconstructed phase-A and -B current values (by DC-bus current sensor, i_{DCM_SCA}) are i_{ARE} and i_{BRE}. Therefore, the relationships among

the scaling errors k_A, k_B, and k_{DC} are

$$\begin{cases} k_A = k_{DC} \cdot i_{AM}/i_{ARE} \\ k_B = k_{DC} \cdot i_{BM}/i_{BRE} \end{cases} \tag{14}$$

The average value of the three scaling errors are given in (15), which can be calculated as k times of k_{DC}

$$\frac{k_A + k_B + k_{DC}}{3} = \frac{i_{AM} \cdot i_{BRE} + i_{BM} \cdot i_{ARE} + i_{ARE} \cdot i_{BRE}}{3 i_{ARE} \cdot i_{BRE}} \cdot k_{DC}$$
$$= k \cdot k_{DC} \tag{15}$$

Therefore, in order to compensate the scaling errors among the current sensors, the compensation coefficients are

$$\begin{cases} k_{DC\_COM} = k = \dfrac{i_{AM} \cdot i_{BRE} + i_{BM} \cdot i_{ARE} + i_{ARE} \cdot i_{BRE}}{3 i_{ARE} \cdot i_{BRE}} \\[3mm] k_{A\_COM} = \dfrac{i_{AM} \cdot i_{BRE} + i_{BM} \cdot i_{ARE} + i_{ARE} \cdot i_{BRE}}{3 i_{AM} \cdot i_{BRE}} \\[3mm] k_{B\_COM} = \dfrac{i_{AM} \cdot i_{BRE} + i_{BM} \cdot i_{ARE} + i_{ARE} \cdot i_{BRE}}{3 i_{ARE} \cdot i_{BM}} \end{cases} \tag{16}$$

where k_{DC_COM}, k_{A_COM}, and k_{B_COM} are the compensation coefficients of DC-bus current sensor, phase-A, and -B current sensors, respectively.

By substituting (14) and (16) into (13), the detected DC-bus and three-phase current values after calibration are

$$\begin{cases} i_{DCM\_CALI} = k_{DC\_COM} \cdot i_{DCM\_SCA} = k \cdot k_{DC} \cdot i_{DC} \\ i_{AM\_CALI} = k_{A\_COM} \cdot i_{AM\_SCA} = k \cdot k_{DC} \cdot i_A \\ i_{BM\_CALI} = k_{B\_COM} \cdot i_{BM\_SCA} = k \cdot k_{DC} \cdot i_B \\ i_{CM\_CALI} = -i_{AM\_CALI} - i_{BM\_CALI} = k \cdot k_{DC} \cdot i_C \end{cases} \tag{17}$$

where i_{DCM_CALI}, i_{AM_CALI}, i_{BM_CALI}, i_{CM_CALI} are the DC-bus and three-phase currents after the mutual calibration of errors.

It can be seen that the scaling error differences among the multiple current sensors in (13) have been compensated in (17). Different from the offset errors that can be precisely eliminated with the proposed calibration strategy, the scaling errors cannot be completely cancelled with the aforementioned scheme. However, the compensation method is able to balance the scaling error differences among all the current sensors, which means that the scaling errors of all the current sensors can be pulled back to the same level. By this means, the negative effects of the scaling error differences on the system, which cause the speed ripple which is two times the fundamental frequency, could be cancelled out [12]. It is also worth noting that the proposed mutual scaling error calibration strategy for the phase current sensors is also applicable for three-phase current sensor based systems.
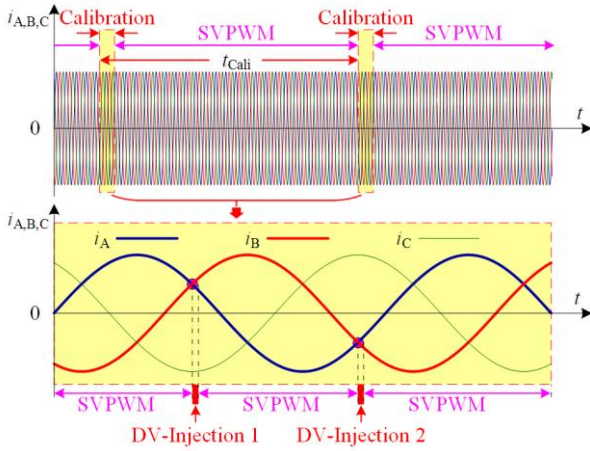
Fig. 3. The proposed detection voltage injection method for mutual calibration of the multiple current sensors.
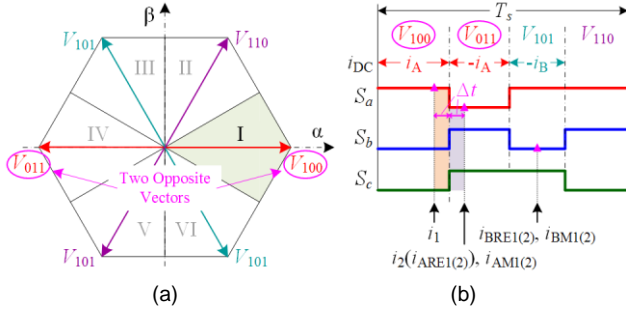

Fig. 4. The DV-Injection process: (a) The divided six sectors, (b) The current sampling strategy (Section I).

IV. OVERALL CONTROL SCHEME

A. Detection Voltage Injection (DV-Injection) Method

In this paper, the detection voltage injection (DV-Injection) method is utilized for mutual calibration of multiple current sensors, as illustrated in Fig.3. The DV-Injection method applies the calibration process during the set intervals t_{Cali} among the commonly used space vector pulse width modulation (SVPWM) process. The interval t_{Cali} is selected according to the running state and environment. In the period of mutual calibration, as shown in the yellowish shading areas, only two DV-Injection points are set, whereas the rest areas are set with SVPWM strategy. In this way, the increase in total harmonic distortion (THD) caused by DV-Injection can be reduced as much as possible.

For the drive with two phase current sensors, e.g., phase-A and -B current sensors, the two DV-Injection points are set at where the two measured currents have the positive and negative values with the same magnitude, respectively, which are indicated as DV-Injection 1 and 2 in Fig.3. The DV-Injection method utilizes the six effective basic voltage vectors (V_{100}, V_{110}, V_{010}, V_{011}, V_{001}, V_{101}) to synthesize the output voltage, and eliminates the two zero vectors (V_{000} and V_{111}) used in SVPWM strategy. In order to apply the proposed DV-Injection strategy, the output voltage range is divided into six brand new sectors that are shown in Fig.4 (a). In each defined sector, the applied vectors and the measured currents are displayed in Table V.

From Table V, it can be seen that six current values can be

TABLE V
THE APPLIED BASIC VECTORS AND MEASURED CURRENTS IN EACH DEFINED SECTOR.

Sector	Basic Vectors	Measured Currents	
		DV-Injection 1	DV-Injection 2
I	V_{100}, V_{110}, V_{011}, V_{101}		
II	V_{100}, V_{110}, V_{010}, V_{001}		
III	V_{110}, V_{010}, V_{011}, V_{101}	i_1, i_2,	i_1, i_2,
IV	V_{100}, V_{010}, V_{011}, V_{001}	i_{ARE1}, i_{BRE1},	i_{ARE2}, i_{BRE2},
V	V_{110}, V_{011}, V_{001}, V_{101}	i_{AM1}, i_{BM1}	i_{AM2}, i_{BM2}
VI	V_{100}, V_{010}, V_{001}, V_{101}		

obtained from the two DV-Injection processes. Take Sector I as an example, the DV-Injection process together with the current sampling strategy can be illustrated in Fig.4 (b). With the proposed DV-Injection and current sampling strategy, all the current values required for current sensor mutual calibration can be obtained at the two DV-Injection points in Fig.3.

Because filters and sampling delays have influence on current sampling, effective current measurements cannot be obtained immediately after vector switching [17]. Therefore, the current sampling point cannot be set instantly after the vector switching point, that is, the action time of each basic voltage vector that needs to be sampled must be maintained for a minimum period of T_{min}. The minimum action time is similar to that required in the phase current reconstruction strategies. As to how to ensure the minimum action time of basic vectors, relevant methods in the phase current reconstruction strategy have already been proposed in [17], and they won't be covered in this paper.

For the current sensor error compensation strategy proposed in this paper, if there exists sampling noise, the measured currents that the compensation strategy depends on will become inaccurate, leading to the deviation of error parameter estimation and compensation. If the influence of the sampling noise needs to be cancelled, the DV-injection process can be repeated for many times in the two injection points in Fig. 3. Therefore, multiple groups of current sensor error parameters can be obtained with the multiple groups of detected currents, and the influence of noise can be counteracted by average algorithm. Considering that the two types of current sensor errors mentioned in this paper change relatively slow with time, the effect of noise can also be counteracted by adding a digital low-pass filter to the estimated sensor error parameters.

B. Closed Loop Control of the System

A common IPMSM drive diagram with the proposed mutual calibration strategy is illustrated in Fig.5. The current sensors and the encoder are installed to obtain the three-phase currents and position/speed information for the dual closed-loop control of current and speed. The current SAU calibration module detects the corresponding current values by issuing the DV-injection switching instruction, and then estimates the types and sizes of the sensor errors according to the proposed algorithm (represented by "Cali. Para." in Fig. 5). Therefore, the current information which contains uncertain errors can be finally detected and calibrated.
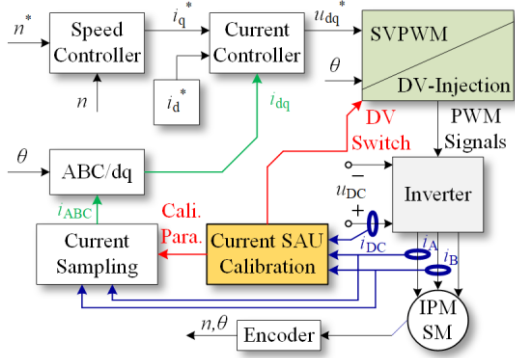
Fig. 5. IPMSM drive diagram with proposed mutual calibration strategy.

TABLE VI
MAIN PARAMETERS OF IPMSM FOR EXPERIMENT.

Parameter	Value	Parameter	Value
Rated power	5 kW	Pole pairs	3
Inverter DC voltage	540 V	d-axis Inductance	4.2 mH
Rated voltage	380 V	q-axis Inductance	10.1 mH
Rated current	8.5 A	Phase resistance	0.18 Ω
Efficiency	0.9	Maximum speed	3000 r/min
Rated torque	15 N·m		

V. SIMULATION VALIDATION

In order to validate the effectiveness of the mutual calibration strategy for multiple current sensors in the drive, simulations have been carried out in MATLAB/Simulink. The main parameters of IPMSM used in both the simulation and experiment are given in Table VI.

The errors of the multiple current sensors are added artificially to the sampling results of the current feedback values. Additionally, in order to test the impacts of actual environmental changes on system performances and the validity of the corresponding mutual calibration strategy in such conditions, the multiple current sensor errors are set as time-varying values rather than constant ones. The variations of different types of errors in multiple current sensors are set to the cases as illustrated in Fig. 6.

The motor starts from 0 to 500 rpm with a load of 15 N·m. At 2.5 s a sudden load of 5 N·m is removed from the motor shaft. At 5 s a sudden load of 5 N·m is added to the motor shaft. At 7.5 s the motor speed is set to 800 rpm. The simulation results of the phase currents without mutual calibration of the multiple current sensor errors are given in Fig. 7. From the simulation results, it can be seen that the actual three-phase currents show unbalanced curves. Whereas the detected three-phase currents are balanced, even when the load and speed are fast changing. This is due to the closed-loop current control of the drive.

In Fig. 8, the simulation results of the torque ripple and speed fluctuation without mutual calibration of the multiple current sensor errors are displayed. It can be seen that the torque ripple is about 5 N·m and the speed fluctuation is 90 rpm, which are obvious and seriously deteriorate the system performance.

In order to eliminate the adverse effects of the current sensor errors, a mutual calibration strategy is proposed. In Fig. 9, the detected current sensor errors are displayed, and it can be seen
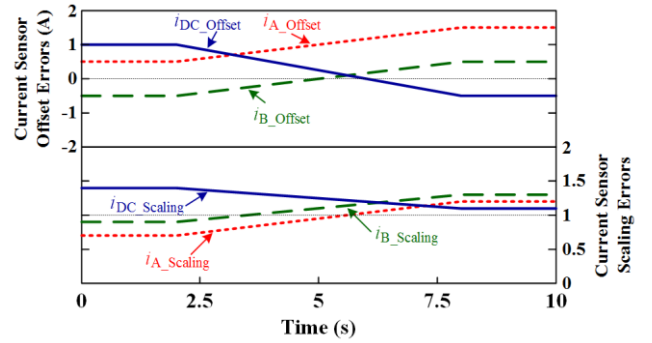

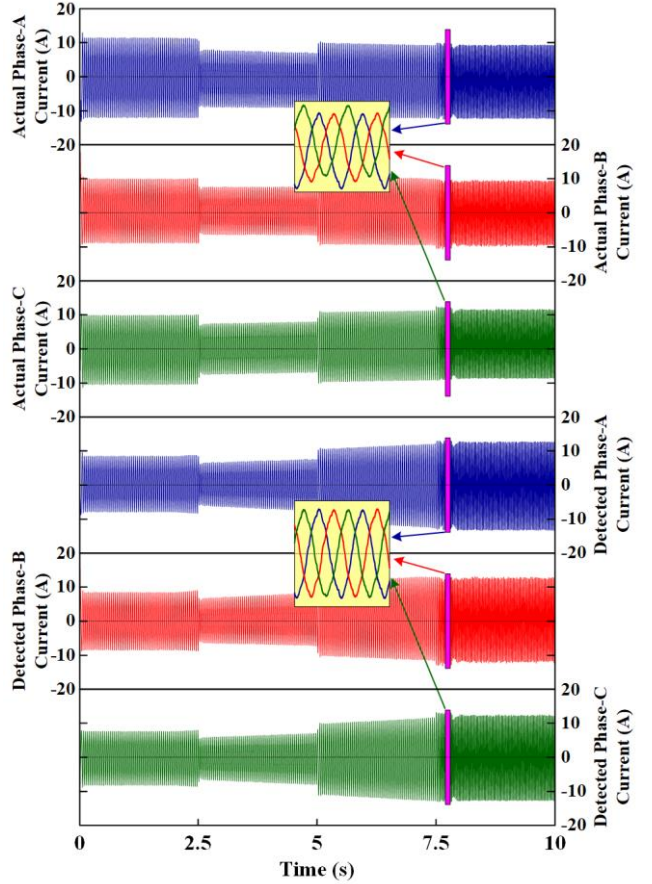Fig. 6. The variations of multiple current sensor errors.

Fig. 7. The simulation results of the phase currents without mutual calibration of the multiple current sensor errors.
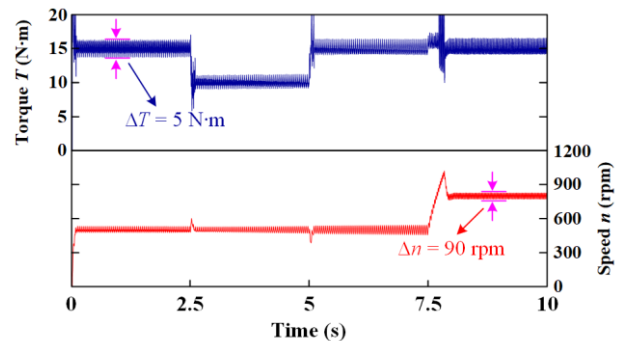

Fig. 8. The simulation results of the torque ripple and speed fluctuation without mutual calibration of the multiple current sensor errors.
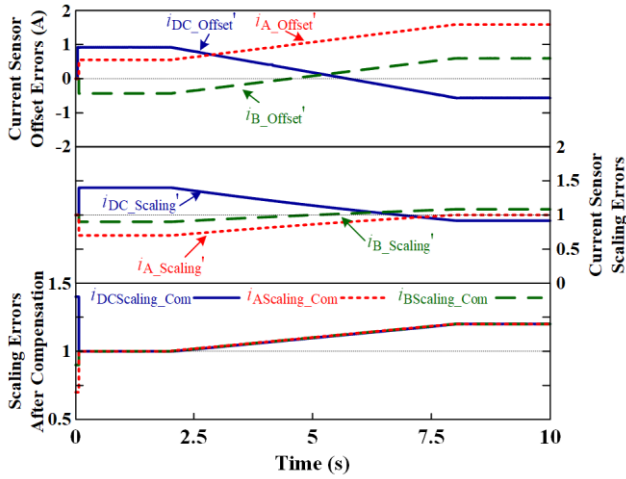
Fig. 9. The detection of multiple current sensor errors.

that the offset errors follow the actual ones accurately in Fig. 6. The overall trends of scaling errors are reproduced in a relatively correct paradigm, but the specific values are not exactly the same as those shown in Fig. 6. However, the absolute scaling errors of the three current sensors are pulled to a same level. This will not only balance the three-phase currents but also greatly reduce the torque ripple and speed fluctuation of the motor, which has been proven in [12].

In Fig. 10, the simulation results of the three-phase currents after mutual calibration of the multiple current sensor errors are given. It can be seen that after applying the mutual calibration process, the actual three-phase currents show very good performances. The actual three-phase current curves are balanced, and the amplitudes of the three-phase currents remain unchanged. After the artificial introduction of the various errors of the current sensors, the waveforms of the detected three-phase currents are distorted greatly. The three-phase current waveforms are no longer balanced, and the amplitudes of the currents change significantly with the speed and load unchanged. After the mutual calibration of the detected currents, the compensated three-phase currents become balanced again. Even when the speed and load are changing rapidly, the current amplitudes do not change significantly, so is the case when the speed and load remain unchanged. The compensated three-phase currents are sent back to the system for current closed-loop control so that the stability of system can be guaranteed.

The simulation results of the torque ripple and speed fluctuation after mutually calibrating the multiple current sensor errors are displayed in Fig. 11. It can be seen that the torque ripple is about 2 N·m and the speed fluctuation is 10 rpm, which are reduced by 60 % and 89 % compared to the values before calibration, respectively. It can be concluded that the torque ripple and speed fluctuation are obviously reduced, and the system performances are greatly improved.

VI. EXPERIMENTAL VALIDATION

In order to further validate the effectiveness of the proposed mutual calibration strategy for multiple current SAU, an experimental platform is set up as shown in Fig. 12. The used
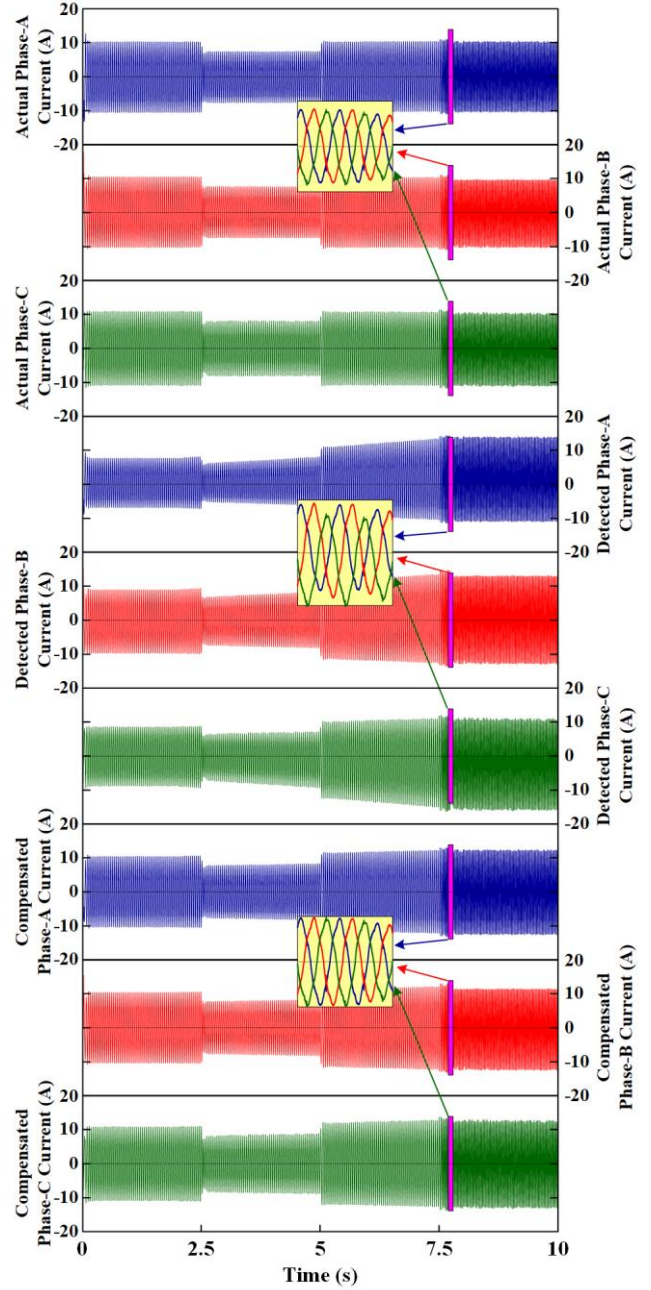

Fig. 10. The simulation results of the phase currents after mutual calibration of the multiple current sensor errors.
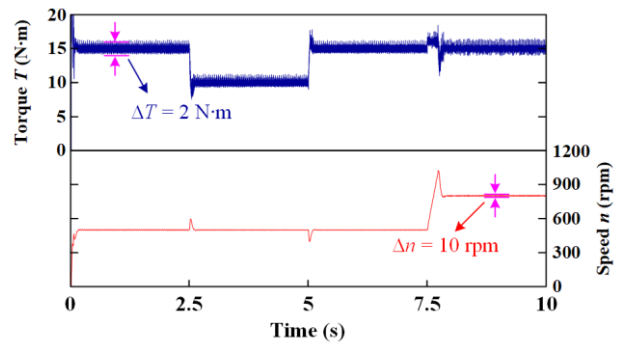

Fig. 11. The simulation results of the torque ripple and speed fluctuation after mutual calibration of the multiple current sensor errors.
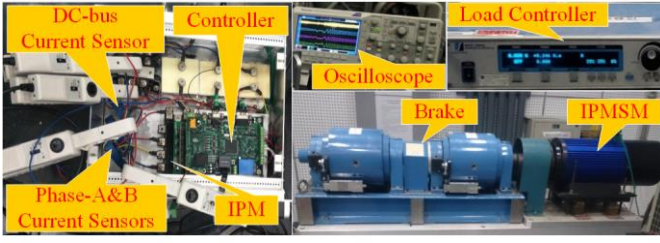
Fig. 12. Experimental platform.

TABLE VII
ERRORS OF DC-BUS AND PHASE CURRENT SENSORS.

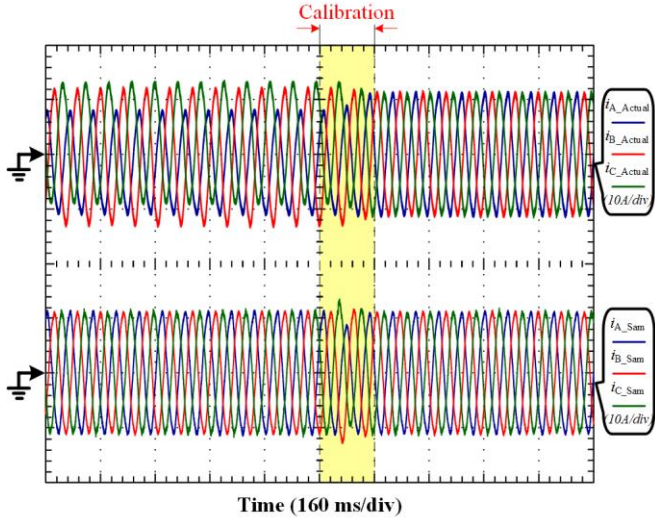| Current Sensors	Offset Errors (A)	Scaling Errors
DC-Bus	-1.0	1.1
Phase-A	1.5	1.2
Phase-B	0.5	0.9

Fig. 13. Experimental results of actual and detected three-phase currents before and after mutual calibration of the multiple current sensors.

current sensors are isolated hall-effect sensors (HS01-100, maximum sample rate 100 kHz). The offset and scaling errors of DC-bus and phase current sensors are added to the software as given in Table VII.

In Fig. 13, the experimental results of actual and detected three-phase currents before and after mutual calibration of the multiple current sensors are presented. In the figure, i_{A_Actual}, i_{B_Actual}, i_{C_Actual} are the actual three-phase currents. i_{A_Sam}, i_{B_Sam}, i_{C_Sam} are the sampled three-phase currents, where i_{C_Sam} is the opposite value of ($i_{A\_Sam} + i_{B\_Sam}$). It can be seen that the actual three-phase currents show unbalanced waveforms before calibration, whereas the sampled three-phase currents are balanced. This is because the sampled currents are the directly controlled signals. After calibration, both the actual and sampled currents return to the state of three-phase equilibrium.

The experimental results of the calibration process are illustrated in Fig. 14. In the figure, DV-Injection 1&2 are the two calibration signal sampling points. The detected currents are given in Table VIII. From Table VIII, it can be seen that the estimated offset error of the DC-bus current sensor is almost the same as the actual one, which also demonstrate the effectiveness of simplifying (1) and (2) into (3) in Section II.
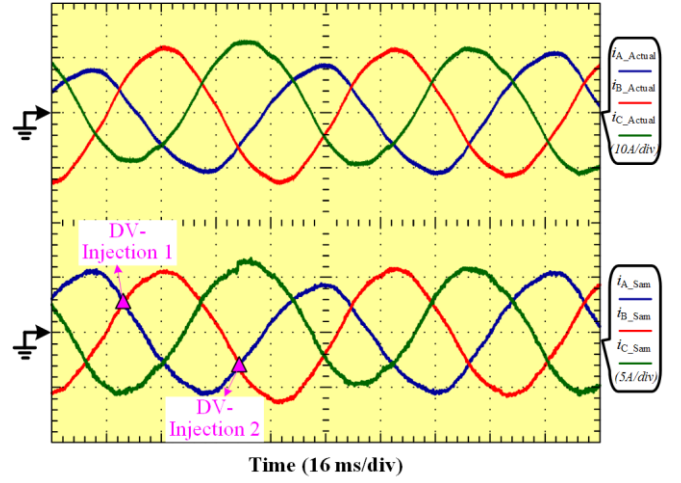

Fig. 14. Experimental results of the calibration process.

TABLE VIII
THE DETECTED CURRENTS IN FIG.14.

DV-Injection 1		DV-Injection 2	
i_1	8.9 A	i_1	14.4 A
i_2	-10.8 A	i_2	-16.3 A
i_{ARe1}	3.6 A	i_{ARe2}	-7.0 A
i_{AM1}	5.5 A	i_{AM2}	-6.2 A
i_{BRe1}	6.1 A	i_{BRe2}	-8.1 A
i_{BM1}	5.5 A	i_{BM2}	-6.2 A
i_{DC_Offset}'	-0.95 A	k_{DC_COM}	0.98
i_{A_Offset}'	1.53 A	k_{A_COM}	0.88
i_{B_Offset}'	0.47 A	k_{B_COM}	1.18
$k_{DC\_COM} \cdot k_{DC}$	1.08	$k_{A\_COM} \cdot k_A$	1.06
$k_{B\_COM} \cdot k_B$	1.06		

After DV-Injection point 2, the errors of the current sensors are detected and calibrated. Additionally, it can be noticed that after the calibration point 2, it still takes a short period of time before the actual three-phase currents become balanced. This is because the actual controlled variables, i.e., the sampled currents, have a step jump after correction.

The experimental results of the torque ripples ΔT before and after calibration are illustrated in Fig. 15, which are 1.5 N·m and 0.3 N·m, respectively. The torque ripple is reduced by 80 % compared to the values before calibration.

The experimental results of the speed fluctuation Δn before and after calibration are illustrated in Fig. 16, which are 4 rpm and 2 rpm, respectively. The speed fluctuation is reduced by 50% compared to the value before calibration.

The frequency spectrum of the speed fluctuation before and after calibration are presented in Fig.17 (fundamental frequency 15 Hz). It can be seen that both the one and two times the fundamental frequency speed fluctuation are reduced after calibration of the current sensor errors. In the figure, 1x and 2x harmonics does not eliminate completely after calibration, this is mainly due to the defective calibration process caused by sampling errors and noise.

The experimental results of the actual and sampled three-phase currents during load and speed change is illustrated in Fig. 18. It can be seen that although the detected three-phase current fluctuates greatly, the actual three-phase current after compensation is balanced.
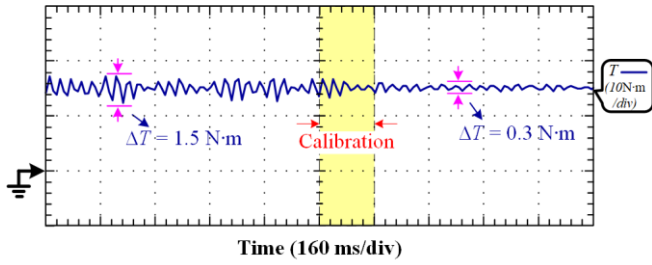
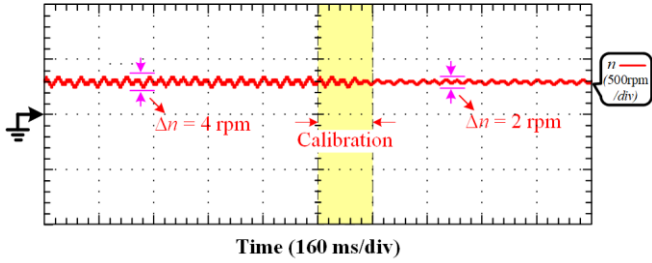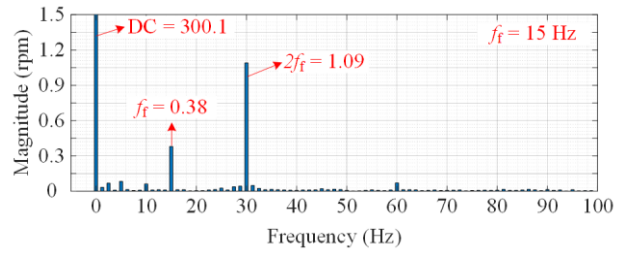Fig. 15. Experimental results of torque ripples.

Fig. 16. Experimental results of speed fluctuation.

Fig. 17. Frequency spectrum of speed fluctuation in Fig.16: (a) before calibration, (b) after calibration.
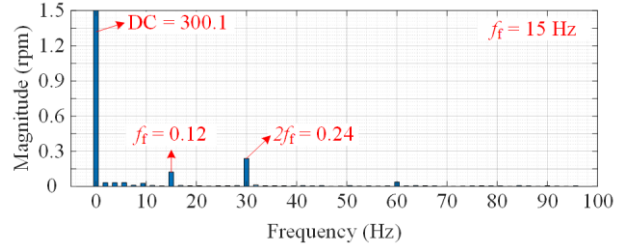
VII. CONCLUSION

The various errors of current sensors in motor driver bring adverse driving experiences to EVs. In order to solve the problem of current sensor accuracy uncertainty caused by aging and harsh working conditions, this paper proposes a mutual calibration strategy for the multiple current sensors. The calibration strategy utilizes a proposed detection voltage injection method, which is simple to implement. The effectiveness of the proposed scheme is verified by the simulation study in MATLAB/Simulink and experimental results on a 5 kW IPMSM motor prototype. The torque ripple is reduced by 60 % in simulation and 80 % in experiment. The speed fluctuation is reduced by 89 % in simulation and 50 % in experiment.

1) The proposed strategy realizes the self-calibration and mutual-calibration of the multiple current sensors with no additional equipment.
2) The calibration process does not need the mathematical model of the motor, but uses the logical relationships among the various current sensors. Therefore, the complex observers and filters are removed from the calibration process.
3) The calibration process is simple and easy to implement, which only utilizes the DV-Injection method at the two injection points. Whereas for the rest of the time, the more commonly applied SVPWM technology is used.
4) The calibration strategy realizes the on-line calibration of multiple current sensors.
5) The effectiveness of the proposed calibration strategy mainly depends on the accuracy of the sampled current values compared to the actual ones. Therefore, the influence of noise on current sampling will increase with the decrease of current level. To obtain a better calibration result, the trigger condition of the currents during calibration strategy should not be at a lower level.
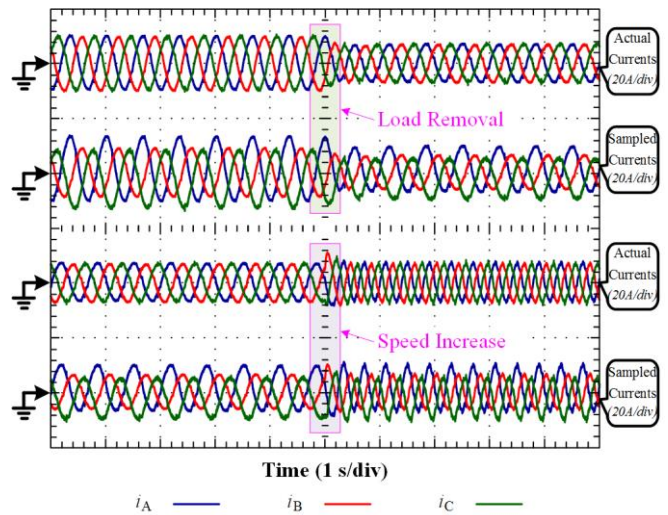
Fig. 18. Experimental results of actual and sampled three-phase currents during load and speed change.

REFERENCES

[1] S. K. Kommuri, M. Defoort, H. R. Karimi, and K. C. Veluvolu, "A robust observer-based sensor fault-tolerant control for PMSM in electric vehicles," *IEEE Trans. Ind. Electron.*, vol. 63, no. 12, pp. 7671 - 7681, Dec. 2016.
[2] Y. H. Hu, C. Gan, W. P. Cao, W. H. Li, and S. J. Finney, "Central-tapped node linked modular fault-tolerance topology for SRM applications," *IEEE Trans. Power Electron.,* vol. 31, no. 2, pp. 1541 - 1554, Feb. 2016.
[3] J. L. Liu, C. Gong, Z. X. Han, and H. Z. Yu, "IPMSM model predictive control in flux-weakening operation using an improved algorithm," *IEEE Trans. Ind. Electron.*, vol. 65, no. 12, pp. 9378 - 9387, Dec. 2018.
[4] Z. Wang, Y. Zheng, Z. Zou, and M. Cheng, "Position sensorless control of interleaved CSI fed PMSM drive with extended Kalman filter," *IEEE Trans. on Magnetics,* vol. 48, no. 11, pp. 3688 - 3691, Nov. 2012.

[5] S. Nalakath, Y. G. Sun, M. Preindl, and A. Emadi, "Optimization-based position sensorless finite control set model predictive control for IPMSMs," *IEEE Trans. Power Electron.*, vol. 33, no. 10, pp. 8672 - 8682, Oct. 2018.

[6] S. N. Vukosavić, L. S. Perić, and E. Levi, "AC current controller with error-free feedback acquisition system," *IEEE Trans. Energy Convers.,* vol. 31, no. 1, pp. 381 - 391, Mar. 2016.

[7] C. L. Xia, P. F. Li, X. M. Li, and T. N. Shi, "Series IGBT chopping strategy to reduce DC-link capacitance for brushless DC motor drive system," *IEEE Journal of Emerging and Selected Topic in Power Electronics*, vol. 5, no. 3, pp. 1192 - 1204, Sep. 2017.

[8] W. T. Deng, C. L. Xia, Y. Yan, Q. Geng, and T. N. Shi, "Online multiparameter identification of surface-mounted PMSM considering inverter disturbance voltage," *IEEE Trans. Energy Convers.,* vol. 32, no. 1, pp. 202 - 212, Mar. 2017.

[9] C. Chakraborty and V. Verma, "Speed and current sensor fault detection and isolation technique for induction motor drive using axes transformation," *IEEE Trans. Ind. Electron.,* vol. 62, no. 3, pp. 1943-1954, Mar. 2015.

[10] F. R. Salmasi, "A self-healing induction motor drive with model free sensor tampering and sensor fault detection, isolation, and compensation," *IEEE Trans. Ind. Electron.*, vol. 64, no. 8, pp. 6105 - 6115, Aug. 2017.

[11] M. Kim, S. K. Sul, and J. Lee, "Compensation of current measurement error for current-controlled PMSM drives," *IEEE Trans. Ind. Appl.*, vol. 50, no. 5, pp. 3365 - 3373, Sep./Oct. 2014.

[12] H. S. Jung, S. H. Hwang, J. M. Kim, C. U. Kim, and C. Choi, "Diminution of current-measurement error for vector-controlled AC motor drives," *IEEE Trans. Ind. Appl.*, vol. 42, no. 5, pp. 1249 - 1256, Sep./Oct. 2006.

[13] Q. N. Trinh, P. Wang, Y. Tang, L. H. Koh, and F. H. Choo, "Compensation of DC offset and scaling errors in voltage and current measurements of three-phase AC/DC converters," *IEEE Trans. Power Electron.*, vol. 33, no. 6, pp. 5401 - 5414, June 2018.

[14] Q. W. Zhai, K. Meng, Z. Y. Dong, and J. Ma, "Modelling and analysis of lithium battery operations in spot and frequency regulation service markets in Australia electricity market," *IEEE Trans. Ind. Informat.*, vol. 13, no. 5, pp. 2576 - 2586, Oct. 2017.

[15] H. Yan, Y. X. Xu, J. B. Zou, Y. Fang, and F. Y. Cai, "A novel open-circuit fault diagnosis method for voltage source inverters with single current sensor," *IEEE Trans. Power Electron.*, vol. 33, no. 10, pp. 8775 - 8786, Oct. 2018.

[16] G. L. Wang, J. Y. Kuang, N. N. Zhao, G. Q. Zhang, and D. G. Xu, "Rotor position estimation of PMSM in low speed region and standstill using zero voltage vector injection," *IEEE Trans. Power Electron.*, vol. 33, no. 9, pp. 7948 - 7958, Sep. 2018.

[17] J. D. Lu, X. K. Zhang, Y. H. Hu, J. L. Liu, C. Gan, and Z. Wang, "Independent phase current reconstruction strategy for IPMSM sensorless control without using null switching states," *IEEE Trans. Ind. Electron.,* vol. 65, no. 6, pp. 4492-4502, June 2018.

[18] G. L. Wang, D. X. Xiao, N. N. Zhao, X. G. Zhang, W. Wang, and D. G. Xu, "Low-frequency pulse voltage injection scheme-based sensorless control of IPMSM drives for audible noise reduction," *IEEE Trans. Ind. Electron.,* vol. 64, no. 11, pp. 8415-8426, Nov. 2017.

[19] J. D. Lu, Y. H. Hu, X. K. Zhang, Z. Wang, J. L. Liu, and C. Gan, "High frequency voltage injection sensorless control technique for IPMSMs fed by a three-phase four-switch inverter with a single current sensor," *IEEE/ASME Trans. Mechatronics*, vol. 23, no. 2, pp. 758-768, Apr. 2018.

[20] Y. Yu, Y. Z. Zhao, B. Wang, X. L. Huang, and D. G. Xu, "Current sensor fault diagnosis and tolerant control for VSI-based induction motor drives," *IEEE Trans. Power Electron.*, vol. 33, no. 5, pp. 4238-4248, May 2018.

[21] M. Manohar and S. Das, "Current sensor fault-tolerant control for direct torque control of induction motor drive using flux-linkage observer," *IEEE Trans. Ind. Informat.*, vol. 13, no. 6, pp. 2824 - 2833, Dec. 2017.

[22] J. D. Lu, Y. H. Hu, and J. L. Liu, "Analysis and compensation of sampling errors in TPFS IPMSM drives with single current sensor," *IEEE Trans. Ind. Electron.,* vol. 66, no. 5, pp. 3852-3855, May 2019.

[23] N. M. A. Freire, J. O. Estima, and A. J. M. Cardoso, "A new approach for current sensor fault diagnosis in PMSG drives for wind energy conversion systems," *IEEE Trans. Ind. Appl.,* vol. 50, no. 2, pp. 1206-1214, Mar./Apr. 2014.

[24] K. Rothenhagen and F. W. Fuchs, "Current sensor fault detection, isolation, and reconfiguration for doubly fed induction generators," *IEEE Trans. Ind. Electron.,* vol. 56, no. 10, pp. 4239-4245, Oct. 2009.

[25] Y. X. Xu, H. Yan, J. B. Zou, B. C. Wang, and Y. H. Li, "Zero voltage vector sampling method for PMSM three-phase current reconstruction using single current sensor," *IEEE Trans. Power Electron.,* vol. 32, no. 5, pp. 3797-3807, May 2017.

[26] D. W. Chung and S. K. Sul, "Analysis and compensation of current measurement error in vector-controlled AC motor drives," *IEEE Trans. Ind. Appl.*, vol. 34, no. 2, pp. 340 - 345, Mar./Apr. 1998.

[27] M. C. Harke and R. D. Lorenz, "The spatial effect and compensation of current sensor differential gains for three-phase three-wire systems," *IEEE Trans. Ind. Appl.*, vol. 44, no. 4, pp. 1181 - 1189, July/Aug. 2008.

[28] S. K. Kommuri, S. B. Lee, and K. C. Veluvolu, "Robust sensors-fault-tolerance with sliding mode estimation and control for PMSM drives," *IEEE/ASME Trans. Mechatronics*, vol. 23, no. 1, pp. 17 - 28, Feb. 2018.

[29] Y. Cho, T. LaBella, and J. S. Lai, "A three-phase current reconstruction strategy with online current offset compensation using a single current sensor," *IEEE Trans. Ind. Electron.,* vol. 59, no. 7, pp. 2924-2933, Jul. 2012.

[30] M. L. Gu, S. Ogasawara, and M. Takemoto, "Novel PWM schemes with multi SVPWM of Sensorless IPMSM drives for reducing current ripple," *IEEE Trans. Power Electron.,* vol. 31, no. 9, pp. 6461-6475, Sep. 2016.
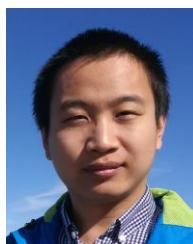
Jiadong Lu (M'19) was born in Pucheng, China, 1990. He received the B.S., the M.S. and the Ph.D. degrees in electrical engineering from Northwestern Polytechnical University (NWPU), Xi'an, China in 2012, 2015 and 2018, respectively. Between 2017 and 2018, he was with the Department of Electrical Engineering, Electronics and Computer Science, University of Liverpool (UoL), U.K. as an Honorary Academic Researcher. Currently, he is an Associate Research Fellow at the Department of Electrical Engineering, NWPU.

His research interests include hybrid-fault-tolerant control techniques for permanent magnet synchronous motor drives, aging issue for motor drives and power electronics converters & control.

Yihua Hu (M'13-SM'15) received the B.S. degree in electrical motor drives in 2003, and the Ph.D. degree in power electronics and drives in 2011. Between 2011 and 2013, he was with the College of Electrical Engineering, Zhejiang University as a Postdoctoral Fellow. Between 2013 and 2015, he worked as a Research Associate at the power electronics and motor drive group, the University of Strathclyde. Currently, he is a Lecturer at the Department of Electrical Engineering and Electronics, University of Liverpool (UoL). He has published 65 papers in IEEE Transactions journals. His research interests include renewable generation, power electronics converters & control, electric vehicle, more electric ship/aircraft, smart energy system and non-destructive test technology. He is the associate editor of IET Renewable Power Generation, IET Intelligent Transport Systems and Power Electronics and Drives.

Guipeng Chen (M'18) received the B.E.E. degree in electrical engineering from Zhejiang University, Hangzhou, China, in 2011, and the Ph.D. degree in power electronics and electric drives from the College of Electrical Engineering, Zhejiang University, in 2017. During the PHD study, he joined Fuji Electric Matsumoto Factory as a summer intern in 2014 and was invited to the University of Liverpool as a research assistant for a half-year program from July 2016. He is currently working as a Postdoc at the Instrument Science and Technology Postdoc Center, School of Aerospace Engineering, Xiamen University, China. His current research interests include automatic topology derivation of dc-dc converters and fault-tolerant converters.

Zheng Wang (S'05–M'09-SM'14) received the B.Eng. and M.Eng. degrees from Southeast University, Nanjing, China, in 2000 and 2003, respectively, and the Ph.D. degree from The University of Hong Kong, Hong Kong, in 2008, all in electrical engineering.

From 2008 to 2009, he was a Postdoctoral Fellow in Ryerson University, Toronto, ON, Canada. He is currently a full Professor in the School of Electrical Engineering, Southeast University, China. His research interests include electric drives, power electronics, and distributed generation. He has authored or coauthored over 80 internationally refereed papers and four books in these areas.

Prof. Wang received several academic awards including IEEE PES Chapter Outstanding Engineer Award, Best Paper Award of International Conference on Electrical Machines and Systems (ICMES), Best Session Paper Award of IEEE Annual Meeting of Industrial Electronics (IECON), and Nanjing Outstanding Paper Award of Natural Science.

Jinglin Liu (M'01) received the B.Eng. degree in electrical engineering from Tsinghua University, Beijing, China, in 1986, and the M.Eng. and the Ph.D. degrees in electrical engineering from Northwestern Polytechnical University, Xi'an, China, in 1990 and 2002, respectively. Since 1994, he has been a Faculty Member with Northwestern Polytechnical University, Xi'an, where he is currently a Professor of Electrical Engineering.

His research interests include electrical machines design and drives, power electronics, fault diagnosis, and motion control.